Design of Zero-Ripple-Current Coupled Inductors with PWM signals in Continuous Conduction Mode

D. Gilabert, E. Sanchis-Kilders, *Senior Member, IEEE,* P. J. Martínez, E. Maset, *Member, IEEE,* A. Ferreres, V. Esteve, *Senior Member, IEEE*

***Abstract*—Coupled inductors are widely used in multiple outputs and interleaved dc-dc converters. Also filters often use coupled inductors as their inductive part. A generalized design procedure is proposed in this paper focused on current ripple minimization and applicable to coupled inductors exposed to PWM signals and in continuous conduction mode. The design provides a very large inductance for all windings but one. Compared to other designs it adapts to the existing magnetic properties of the magnetic device changing only the inductance ratio, simplifying the design and manufacturing process. It is based on the equivalent inductance value and its divergences. The only assumption applied is that the coupling coefficient among all windings is the same, which is an acceptable approximation in many magnetic core architectures. The theoretical results are experimentally verified. Not only almost zero ripple current is achieved, but also mass and volume is reduced compared to non-coupled inductors. This is an additional advantage of coupled inductors in mass and volume critical applications, like aerospace.**

***Index Terms*—inductors, magnetic device, zero ripple current**

I. Introduction

COUPLED Inductors (CI) are widely used as magnetic parts in multiple outputs converters [1]–[5]. Also filters use CI [6]–[8] to improve their frequency rejection adding a notch but the proposed design cannot be easily applied to power converters and is focused on two windings CI. Space applications make extensive use of CI [9]–[13] mainly due to the mass and volume reduction. To the reduction of mass and volume, many more advantages have been reported in technical literature. In fact, in [4] not only a current ripple reduction is stated, but also lower cross regulation is claimed. Stability improvement of CI have been demonstrated in [14], [15]. The current ripple reduction is of great advantage when feeding microprocessors, to reduce the capacitor bank as shown in [16]. An experimental comparison of CI and single inductors can be found in [17] and [18], but without providing too much mathematical insight.

In ac applications, a reduction of THD is also demonstrated [19] and a losses decrease is claimed due to the current ripple and volume reduction of the CI in [20]. Other ac converters using a CI and proposing a symmetrical magnetic design have been reported in [21]. This symmetrical design assures an almost equal coupling coefficient for all windings, that could be applied in the hereafter proposed design procedure.

But all these articles are focused on the converter itself and the proposed magnetic design cannot be easily applied to other converters.

One of the first studies that analyzed zero-ripple-current (ZRC) in CI is [22]. It chooses the coupling coefficient equal to the turns ratio, statement that agrees with the idea of this paper. But to fulfill this equality it varies the gap of the magnetic element. Whereas, the hereafter proposed design procedure moves the divergence responsible of the ZRC condition to the already existing real coupling coefficient value by just changing the inductance ratio, greatly simplifying the design of the ZRC CI.

Other designs couple identical inductors together, missing the influence of their value or turns ratio [22] in the ZRC condition. Although they present the influence of the duty cycle in the current ripple, they risk the appearance of additional time intervals that can distort the current ripple severely by changing the voltage levels applied to CI. Correcting this voltage level change is not always possible, as it affects the output voltage. In [23]–[25], current ripple is reduced adjusting the coupling coefficient, as proposed in our work, to enhance the battery life when used for charging and discharging. But these papers don't provide general design procedures or general mathematical equations that could allow using their design procedure in other applications.

Many papers apply finite element analysis (FEA) to analyze magnetic elements, like in [26]–[28] that present an optimum *ad-hoc* design, which, once more, is difficult to use in other applications. In [29] the CI is also analyzed thoroughly including a FEA, this time focused on an interleaved dc-dc converter. It is true that FEA provides a very precise magnetic design but it strongly depends on the FEA grid, its symmetry and therefore on the chosen core and winding geometry. Although the results can be very precise, they are case by case solutions.

Either the design techniques of CI found in technical liter-

Manuscript received June 17; revised August 1 and October 4; accepted December 14, all 2019. This work has been partially funded by the Spanish Ministerio de Economía, Industria y Competitividad and Ministerio de Ciencia Innovación y Universidades through Projects ESP2014-56169-C6-4-R, ESP2016-77548-C5-5-R and RTI2018-096886-B-C54 including a percentage from European FEDER funds.

All authors are with the Dpt. of Electronic Engineering, University of Valencia, 46100 Burjassot, Spain; (corresponding author e-mail: esteban.sanchis@uv.es).

ature are *ad-hoc* designs that optimize a particular application or the design techniques are focused on optimized geometrical magnetic designs that are very difficult to generalize.

The only generalized CI description that explains the reason for ZRC condition found so far is [30]. Based on this CI analysis hereby we propose a design technique for CI that directly leads to ZRC, reducing mass and volume as well. It can be applied to any type of converter that applies PWM waveforms in continuous conduction mode (CCM) to a CI.

The magnetic properties of the core together with the winding strategy are considered but the proposed solution does not require special magnetic design techniques. Just classical design techniques applied in a special manner, and explained in the paper, achieve ZRC. The proposed design procedure assumes that second order effects like core and copper losses are small enough to be negligible.

A. Equivalent Inductance

One condition usually applied and found in technical literature for a CI, [18], is that the ratio between the square-root of its inductances is equal to the ratio between its applied voltages. This assures the volts-second balance of the magnetic element.

Having two windings a and b, this means

$$\sqrt{\frac{L_a}{L_b}} = \frac{v_{L_a}}{v_{L_b}} \tag{1}$$

L_a and L_b are the inductances and v_{L_a} and v_{L_b} are the voltages applied to inductors a and b of the CI.

If (1) is not fulfilled, then the CI suffers an unbalance, which can lead to a bizarre behavior of its current waveforms, but can also be used to achieve ZRC.

This behavior has already been described in [18] and [31], but no mathematical expressions describing these current waveforms have been given. The described CI are also designed for particular cases like having all the same inductance and coupling only two or three inductors together. On the other hand a detailed explanation of this effect together with a comprehensive mathematical analysis can be found in [30].

The change of current ripple experienced by CIs can be directly related to a change of the equivalent inductance of each winding [30], [32]. Therefore, designing the equivalent inductance results in the desired current ripple.

As explained in [30], the unbalance can be used to design a ZRC CI and the optimal design procedure will be presented hereafter. The design is based on the general equivalent inductance expression of a CI exposed to PWM voltage signals and in CCM.

$$\mathbf{L}_{eq} = \left(\mathbf{N}_d^{-1} \cdot \mathbf{L}^{-1} \cdot \mathbf{N}\right)^{-1} \tag{2}$$

Following the same procedure explained in [30] to transform (2) into a more useful expression, all coupling coefficients among windings are supposed the same and equal to $\tilde{k}$. This approximation introduces only a small error if all the elements of matrix $\mathbf{k}$ are very similar. In fact, if the elements of matrix $\mathbf{k}$ are varied about 5 % from each other and we compare the resulting equivalent inductances, we can verify that the results obtained with (2) and (3) differ at most 10 %.

Normalizing all elements of (2) with its corresponding self inductance ($\overline{L_{eq_q}} = \frac{L_{eq_q}}{L_{qq}}$) and operating on them, results in the following simplified expression for the equivalent inductance,

$$\overline{L_{eq_q}} = \frac{\left[(m-1)\tilde{k}+1\right](1-\tilde{k})}{\left[(m-2)\tilde{k}+1\right] - \tilde{k}\sum\limits_{\substack{r=1\\r\neq q}}^{m}\Delta_{qr}} \tag{3}$$

Where Δ_{qr} is the deviation between the q-th and r-th inductors, provoked by unbalances. Its ideal value is 1.

$$\Delta_{qr} = \sqrt{\frac{L_{qq}}{L_{rr}}}\frac{v_{L_r}}{v_{L_q}} \tag{4}$$

Eq. (3) will tend to infinity when the denominator becomes zero.

Fig. 1 represents the normalized equivalent inductances and their variation as a function of the coupling coefficient. It can be clearly seen that in this particular case, a divergence appears around $\tilde{k} \approx 0.95$. Although not shown here, if the unbalance increases, then the divergence moves to lower values of $\tilde{k}$.

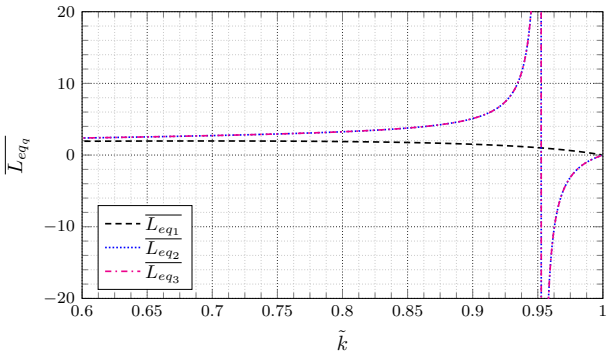

Fig. 1. Normalized equivalent inductances for $L_{11} = 9\mu H$, $L_{22} = 2L_{11}$ and $L_{33} = 4L_{11}$ and applying the voltage $v_{L_{1on}} = 5V$ and choosing the other voltages following (1). The unbalance chosen for the real expression is 10 % for L_{22} and L_{33}. We suppose that all coupling coefficients are the same.

There are three different ways to move the divergence, which is the pole of (3) and depends on the number of windings m: change either the coupling coefficient $\tilde{k}$, or the inductance ratio $\sqrt{\frac{L_{qq}}{L_{rr}}}$ or the voltage ratio $\frac{v_{L_r}}{v_{L_q}}$ as seen in (3) and (4). Changing the coupling coefficient is complicated and has a limited range because it depends on winding strategies and the permeability. But the other two changes are easier to perform. Usually the output voltage level is fixed, so the best option is to change the self-inductance ratios.

B. Zero-ripple-current condition

As proposed in [30], the approach taken in this work is to control the divergence (pole) of (3) for all windings to almost match it with the real coupling coefficient of the magnetic element. For the sake of clarity, the expressions are repeated hereafter. The divergence of the equivalent inductance is

$$\tilde{k}_{divergence_q} = \frac{1}{\sum_{\substack{r=1 \\ r\neq q}}^{m} \Delta_{qr} + 2 - m} \tag{5}$$

As $\tilde{k} < 1$, the following condition assures the existence of a pole,

$$\sum_{\substack{r=1 \\ r\neq q}}^{m} \Delta_{qr} > m - 1 \tag{6}$$

For a given number of windings, m, we can change Δ_{qr} to move the pole. The expression of Δ_{qr} applying the previous assumptions is,

$$\Delta_{qr} = \frac{v_{L_r}}{v_{L_q}}\sqrt{\frac{L_{qq}}{L_{rr}}} = \frac{\sqrt{L_{qq}}}{v_{L_q}} \Big/ \frac{\sqrt{L_{rr}}}{v_{L_r}} \tag{7}$$

Taking into account that $\Delta_{qr} = 1/\Delta_{rq}$, (5) and (6), it can be deduced that a divergence exists in all windings but one winding (for example, the first) and that ZRC can be expected in all windings but one winding (for example, the first).

As the voltages are difficult to change because they are fixed by the circuit, we will change the inductances to move the divergence to the required coupling coefficient $\tilde{k}$. The required $\tilde{k}$ is determined by the expected real coupling coefficient, k_{real}, of the manufactured CI.

The equivalent inductance can be recalculated, taking into account that the ideal value of $\Delta_{qr\,ideal} = 1$, keeping L_{11} as the ideal reference value and changing the values of all other inductances by the same percentage ε.

$$\Delta_{1r} = \sqrt{\frac{L_{11}}{L_{rr}(1+\varepsilon)}}\frac{v_{L_r}}{v_{L_1}} = \Delta_{1r\,ideal}\frac{1}{\sqrt{(1+\varepsilon)}} \tag{8}$$

Using (8) in (3) results,

$$\overline{L_{eq_1}} = \frac{[(m-1)\tilde{k}+1](1-\tilde{k})}{(m-2)\tilde{k}+1-\tilde{k}(m-1)(\frac{1}{\sqrt{1+\varepsilon}})} \tag{9}$$

Now, as $\Delta_{r1} = \Delta_{r1\,ideal}\sqrt{1+\varepsilon}$ and for the other windings no deviation is present, then for these indices $(q, r \neq 1 \wedge q \neq r)$ $\Delta_{qr} = 1$, and we get

$$\overline{L_{eq_q}}\Big|_{q\neq 1} = \frac{[(m-1)\tilde{k}+1](1-\tilde{k})}{1-\tilde{k}(\sqrt{1+\varepsilon})} \tag{10}$$

Fig. 2 shows how the divergence changes with different $\tilde{k}$ values depending on the value of ε. But this figure also tells us how much the normalized value of the equivalent inductance increases. For example, for $\varepsilon = 0.2$, if the coupling coefficient is $\tilde{k} = 0.9$ then $\overline{L_{eq_q}}\big|_{q\neq 1}$ becomes 20 times larger.

The divergence of (10) is therefore,

$$\tilde{k}_{divergence} = \frac{1}{\sqrt{1+\varepsilon}} \tag{11}$$

Thus, changing the values of all inductances but L_{11} by the same percentage ε, in order to not fulfill (1) results in different equivalent inductances. If ε is chosen to comply with (11),

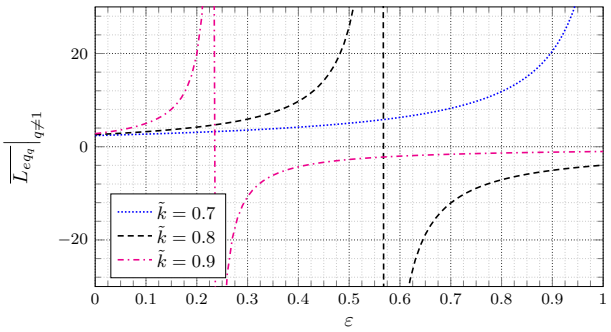

Fig. 2. Variation of the normalized equivalent inductance (10) depending on the deviation ε and the coupling coefficient $\tilde{k}$ for $m = 3$.

then $\overline{L_{eq_q}}\big|_{q\neq 1} \to \infty$ and will reach ZRC at the corresponding outputs. But L_{eq_1} will usually reduce its value as seen in Fig. 3.

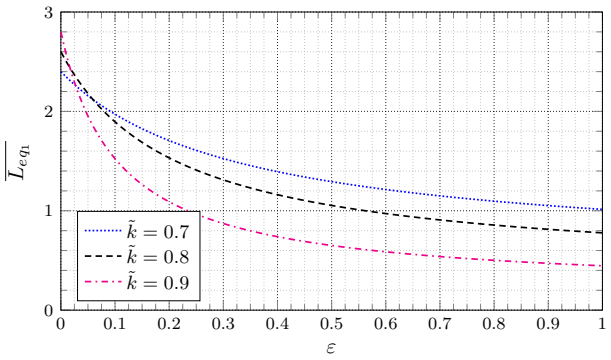

Fig. 3. Change of the reference inductance L_{eq_1} (9) depending on the deviation ε and the coupling coefficient $\tilde{k}$ for $m = 3$.

II. ZRC CI Design Methodology

The design will be valid for any CI exposed to PWM signals and assuming that the currents through all its windings are in CCM. ZRC will be achieved by moving the divergence to the coupling coefficient expected to be obtained with the real CI.

Applying classical inductor design techniques and the aforementioned conditions results in the following procedure.

1) First, if all current ripples are known, then the different inductance values that will be coupled together have to be calculated. Knowing the voltage across each winding, it has to be checked if the values fulfill (1).
2) Usually (1) won't be fulfilled and then we have to choose one inductance as the reference and size the other inductances accordingly to fulfill (1). If current ripples are unknown, then one has to be fixed and it will correspond to the reference inductance. The other inductances, which will have ZRC, have to be calculated based on (1).
3) Now all the inductances, but the reference will be increased to unbalance (1) to achieve ZRC in all inductances, but the reference. This will move the divergence to lower values of $\tilde{k}$. If we know the expected real coupling coefficient, k_{real}, based on our intended winding strategy and the selected core, then we can choose the percentage, ε, that all inductances have to be increased to match

this coupling coefficient using (11) or Fig. 2. A good practice is to keep the divergence, $\tilde{k}_{divergence}$, slightly above the real value k_{real}. The reduction of $\overline{L_{eq_1}}$ must also be checked, either with (9) or with Fig. 3 to keep its current ripple within reasonable values.

4) The energy stored in the magnetic device, (Li^2), determines the core size of the CI and therefore the dc current level, i_o, has to be known. Then a classical magnetic design procedure follows to calculate the required core using, for example, the area-product.
5) Now the design has to achieve the required coupling. For example, if a toroidal core is chosen, then the windings have to be laid out in a way to achieve the desired coupling among them. A low coupling ($k_{real} = 0.8$) means that the windings have to be distributed on different sectors of the torus. It must be taken into account that the core permeability also influences the coupling. For EE or EI cores, an optimal gap has to be designed to achieve the desired coupling, as explained in [24].
6) Depending on the operating frequency and the maximum dc and ac currents, the needed copper area for each winding has to be selected. Thus, one can determine the minimum needed window area of the core. If a toroidal core with a sector distribution of windings is chosen, the window area is the most critical aspect to fulfill.
7) The maximum flux density (B) has to be checked to assure that the core does not saturate.

Finally, the CI has to be measured (see [33]) to check if the requirements are met.

A flow chart of the proposed procedure is shown in Fig. 4.

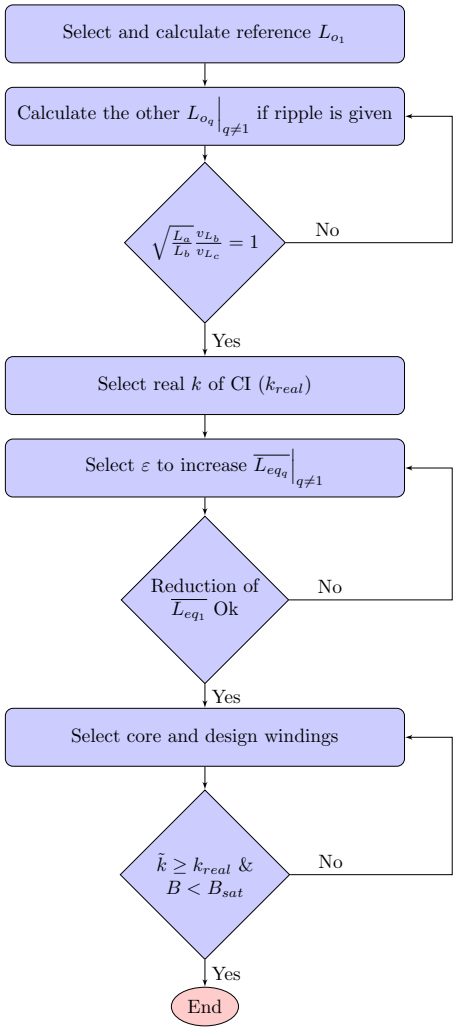

Fig. 4. Flowchart of design procedure.

III. Practical design of a three windings CI

To verify the proposed design methodology a three output Buck converter will be designed following the experimental set-up of [30]. Its three outputs will use a common CI working in CCM where two outputs will have ZRC, and one not.

The specifications of the three different Buck converters are summarized in Table I, where current ripple of outputs 2 and 3 is the maximum value. Even lower values are desirable.

TABLE I
Specifications of three Buck converters with CI

Output	V_{out} (V)	$I_{o_{max}}$ (A)	$I_{o_{min}}$ (A)	V_s (V)	ΔI_L (A)
1	3.3	1.0	0.5	8.25	0.30
2	5	0.5	0.2	12.5	0.02
3	12	0.5	0.2	30.0	0.05

Duty cycle has been limited to $D = 0.4$ and the switching frequency has been chosen to be $f_0 = 100\,\text{kHz}$.

We start with step 1). The required inductance L_o for the three Buck converters together with the critical inductance L_c (limit between CCM and DCM) are shown in Table II and have been calculated using (12) and the values found in Table I,

$$L_o = \frac{V_s(1-D)D}{\Delta I_L f_o}$$
$$L_c = \frac{(1-D)V_{out}}{2I_{o_{min}} f_o} \tag{12}$$

TABLE II
Calculated nominal and critical inductances of the three Buck converters with CI.

Output	$L_c(\mu H)$	$L_o(\mu H)$
1	19.8	66.0
2	75.0	1500
3	180.0	1400

The values shown in Table II already suggest that we need almost ZRC at outputs 2 and 3.

A. ZRC CI design

First we have to adjust voltages and inductances to fulfill (1). Afterwards we have to follow step 2). If we use the inductance of output 1 as reference inductance, then we have

TABLE III
SELF INDUCTANCES TO DESIGN FOR THE REDUCED CI.

$L_{11}(\mu H)$	$L_{22}(\mu H)$	$L_{33}(\mu H)$
66	219.7	1265

TABLE IV
CHARACTERISTICS OF CORE AND WINDINGS OF THE DESIGNED CI.

core	perm. μ	mass (g)	vol. (cm^3)	turns N_{11}	turns N_{22}	turns N_{33}	k
55310	125	16	3.7	27	48	115	0.80

to recalculate the inductances of outputs 2 and 3 to fulfill (1). These new values are $L_{11} = 66\,\mu$H, $L_{22} = 151.5\,\mu$H and $L_{33} = 872.7\,\mu$H.

It is clear now that the required current ripple will not be achieved in outputs 2 and 3 and we will apply step 3) to reach larger inductance values in those outputs.

If we use a toroidal MPP core and wind the three windings on different sectors as shown in the Fig. 6, we can expect a coupling among the windings of $k_{real} \approx 0.8$. The rate (percentage ε) that L_{22} and L_{33} have to change can be calculated using (11). If we want to place the divergence above the real coupling coefficient, $k_{real} \approx 0.8$, we could provide a small margin to $\tilde{k}_{divergence}$, in this case it is approximately 4 %. This will cope with the tolerances of the magnetic device (permeability change, final real coupling, etc.) and in addition it will lower the value of L_{11} less. In this case, a deviation of $\varepsilon = 45$ % has been chosen which based on (11) places the divergence at $k_{divergence} = 0.83$, above the real coupling, $k_{real} \approx 0.8$. Fig. 2 shows that the equivalent inductances will be about 14 times larger and the reference inductance will be about 1.1 times larger, as seen in Fig. 3.

Table III shows the new values of L_{22} and L_{33} which have been increased by 45 %.

Using (3), we can calculate the expected equivalent inductances.

$$\begin{aligned} L_{eq_1} &= 81.1\,\mu\text{H} \\ L_{eq_2} &= 3.1\,\text{mH} \\ L_{eq_3} &= 17.9\,\text{mH} \end{aligned} \tag{13}$$

In case these values are not acceptable, then ε has to be readjusted, even though the tolerances makes it difficult to reach the exact desired values. The current ripple of output 2 will be reduced by a factor of two and the one of output 3 by a factor greater than ten, when comparing L_o of Table III and (13).

B. Core selection

The selected core material will be MPP and the core shape will be toroidal. This type of cores are ideal to save space and volume and offer a wide range of permeabilities to withstand large flux densities without saturating.

Following step 4 of the proposed design procedure and using data given in Table III and Table I, the total energy stored in the core is $E_{total} = 0.5\,\text{mJ}$. Based on the datasheet of the manufacturer (the authors have chosen Magnetics), the maximum flux density for MPP material is $B_{max} = 0.8\,\text{T}$ and the smallest core to handle this energy is #55117 that has an inner diameter of $9.52\,\text{mm}$.

The wires have been chosen based on the current flowing through them (see Table I). At least one wire is needed with a minimum diameter of $0.5\,\text{mm}$ for the large current output and the other two outputs need two wires with a minimum diameter of $0.35\,\text{mm}$.

As explained in step 5), to achieve a lower coupling, k_{real}, the windings have to be distributed in sectors around the torus and the distance from one sector to another makes the coupling larger or smaller. It has to be taken into account that permeability also influences the coupling coefficient. In our case and with a permeability of $\mu = 125$, a separation of $4\,\text{mm}$ between sectors, results in a coupling of $k_{real} \approx 0.8$ (see Fig. 6). A lower coupling than $k_{divergence}$ is preferred as slopes are softer and therefore it is less critical to achieve and keep ZRC (see Fig. 2).

In step 6) we have to check if the available window area is enough for the needed windings. Thus, knowing the needed inductances and the turn-inductance, A_L, of the core, we can calculate the turns number. This allows us to evaluate the needed window area and it can be demonstrated, that the selected window is too small, because we have to wind in sectors to achieve a coupling of $k_{real} \approx 0.8$. The needed window area is $A_w = 28\,\text{mm}^2$ and therefore we select a bigger core #55310 (inner diameter of $13.3\,\text{mm}$). Table IV summarizes the mechanical specifications of the CI to be manufactured.

The last step 7) requires to calculate the flux density, B, of the core to assure that it doesn't saturate. The magnetic field, H, defined by (14), is calculated using the turn number N, the peak current $I_{pk_{max}}$ (see Table I) and the magnetic path length l_e.

$$H = \sum \frac{N I_{pk_{max}}}{l_e} \tag{14}$$

With this calculated value of $H = 19.6\,\text{A/cm}$, the flux density, B can be read from the hysteresis curve of the magnetic material. The resulting flux density results,

$$B_{total} = 0.29\,\text{T} \tag{15}$$

which is well below the saturation flux given by the manufacturer for MPP material $B_{max\ MPP} = 0.8\,\text{T}$.

IV. EXPERIMENTAL RESULTS

Using the same set-up described in [30] (see Fig. 5) to check the proposed design procedure and having the specifications of the converter shown in Table I, the obtained results are explained here after.

The characterization of the CI is done as described in [33]. The measured self-inductances and the coupling matrix are shown in (16) and (17) respectively.

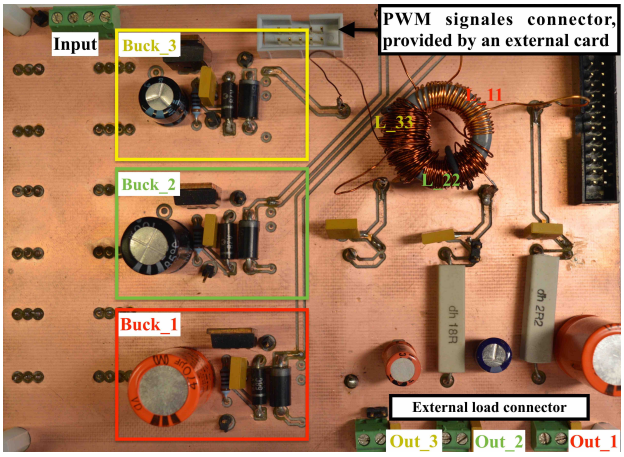

Fig. 5. Experimental set-up. Three BUCK converters sharing their three output inductors, coupled together.

$$\begin{aligned} L_{11} &= 67.58\,\mu\text{H} \\ L_{22} &= 223.47\,\mu\text{H} \\ L_{33} &= 1253\,\mu\text{H} \end{aligned} \tag{16}$$

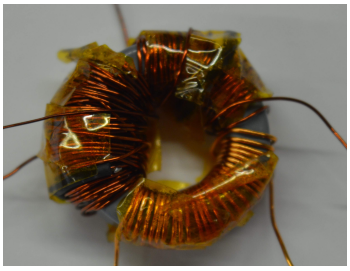

Fig. 6. Coupled inductor manufactured by sectors, the core is #55310 of Magnetics and its coupling is $k_{real} \approx 0.8$.

$$\mathbf{k}_{real} = \begin{pmatrix} 1 & 0.79 & 0.8 \\ 0.79 & 1 & 0.8 \\ 0.8 & 0.8 & 1 \end{pmatrix} \tag{17}$$

It can be seen that the desired coupling has been achieved and that the approximation supposing that all coupling coefficients are very similar is also correct. Using weigh MKS Euro Products, that has a precision of $\pm 0.2\,\text{g}$, the mass of the CI has been determined to be $23.6\,\text{g}$. The volume of the CI has been estimated to be $7.1\,\text{cm}^3$.

A. Experimental measurements, current ripple and output voltages.

The built Buck converter, operated in open loop, has been tested with three loads at each output. Nominal loads, $R_{L_1} = 4.1\ \Omega$ at output 1, resulting in a current of $0.8\,\text{A}$ and for outputs 2 and 3 the loads are $R_{L_2} = 10\ \Omega$ and $R_{L_3} = 36\ \Omega$, where their currents are $0.5\,\text{A}$ and $0.34\,\text{A}$ respectively. Also maximum and minimum loads have been tested, not appreciating any change neither in the current ripple nor in the inductors voltage, as shown in the corresponding figures.

Now the current ripples will be measured to determine the equivalent inductance of each output using $L = \frac{\Delta t\ v_L}{\Delta i_L}$. The measured inductances will be compared to the desired ones given by (2) using measured matrix $\mathbf{k}_{real}$ and (3) and supposing all coupling values equal to $k_{real} = 0.8$.

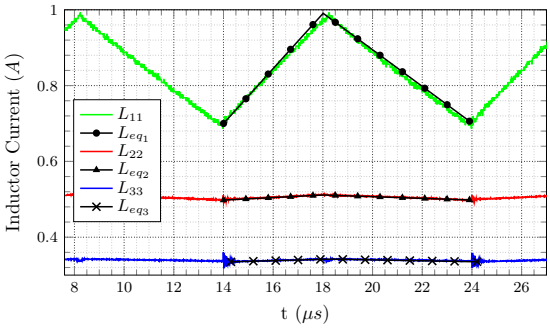

Fig. 7. Measured and calculated (dotted lines, using (2)) current waveforms for nominal conditions of the three coupled BUCK converters. ZRC is achieved in L_{22} and L_{33} and ripple of L_{11} is larger because the value of L_{11} has decreased (although, not seen here).

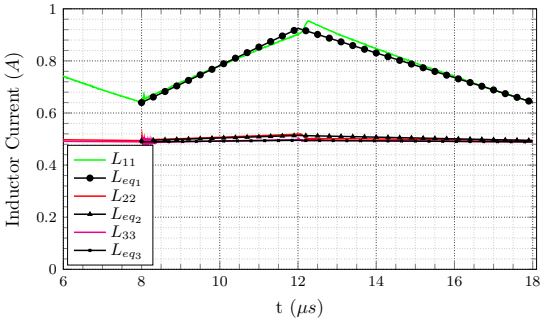

Fig. 8. Measured and calculated (dotted lines, using (2)) current waveforms for maximum conditions of the three coupled BUCK converters.

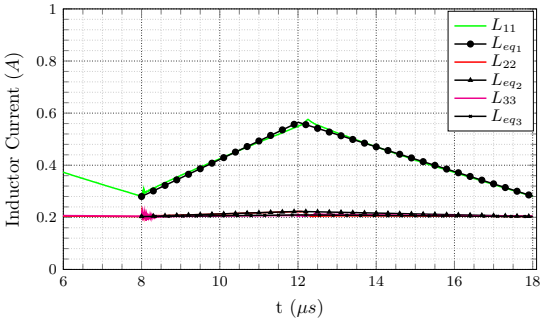

Fig. 9. Measured and calculated (dotted lines, using (2)) current waveforms for minimum conditions of the three coupled BUCK converters.

Fig. 7 shows the current ripple of all three outputs. As expected, the current ripple of L_{22} and L_{33} is close to zero and the ripple of L_{11} is still present. In fact, it will be larger than before unbalancing L_{22} and L_{33}. Table V and VI show the measured and theoretical inductance values.

Fig. 8 and Fig. 9 also clearly show that load does not affect the ZRC condition, which is maintained. This, of course,

TABLE V
MEASURED EQUIVALENT INDUCTANCES

	up ramp	down ramp
L_{eq_1} (μH)	74.0 ± 2.5	73.8 ± 2.5
L_{eq_2} (μH)	2533 ± 122	2658 ± 122
L_{eq_3} (μH)	10249 ± 538	13590 ± 538

TABLE VI
EQUIVALENT INDUCTANCES USING THE MATHEMATICAL MODEL

	Eq. (2) up ramp = down ramp	Eq. (3) up ramp = down ramp
L_{eq_1} (μH)	76.0	74.5
L_{eq_2} (μH)	2974	3060
L_{eq_3} (μH)	13250	9890

means also that the permeability has almost not changed with load.

It is therefore demonstrated that ZRC can be reached in $(m-1)$ windings.

B. Comparison of ZRC CI to single inductors.

This section will compare a design using three single inductors to the proposed CI. The three single inductors will be designed using the experimental values shown in Table V and their mass and volume has been estimated theoretically.

The selected cross-section of the wires are the same as before.

The energy stored in L_{11} is $E_1 = 0.125\,\mathrm{mJ}$. Using again Magnetics, the best fitting core is #55127. The mass of the finished inductor is $2.8\,\mathrm{g}$ and its volume is $0.73\,\mathrm{cm}^3$.

The energy stored in inductor L_{22} is $E_2 = 0.664\,\mathrm{mJ}$, which leads to choose core #55117 of Magnetics. Its mass and volume have been estimated as $9.7\,\mathrm{g}$ and $2.34\,\mathrm{cm}^3$.

Finally, for inductor L_{33} the energy stored is $E_3 = 3.4\,\mathrm{mJ}$. The chosen core based on Magnetics' core selection chart is #55310. Its mass and volume have been estimated as $24.9\,\mathrm{g}$ and $5.6\,\mathrm{cm}^3$.

The total mass and volume are thus $37.5\,\mathrm{g}$ and $8.7\,\mathrm{cm}^3$. This means that a single inductor design has a $59\ \%$ more mass and a $22.5\ \%$ more volume. Therefore, the mass and volume savings of a CI designed with the here proposed methodology, makes it the best choice for mass and volume critical applications, like, for example, aerospace.

An additional advantage not mentioned before is a core loss reduction due to a core mass reduction of the CI. A theoretical loss estimation shows that core losses are reduced by a factor of approximately four.

V. CONCLUSIONS

A practical design procedure of CI has been proposed, based on a general expression proposed for the equivalent inductance of each winding of a CI and the simpler expression of the equivalent inductance when supposing all coupling coefficients to be the same among all the windings.

The proposed design procedure achieves ZRC in the CI. This has been done by only unbalancing the inductance ratio. In fact, for an m windings CI, ZRC is achieved in $m-1$ windings. The design does not need a given coupling coefficient, but it adapts to the real coupling coefficients related to the geometry and permeability of the magnetic device. Therefore complex magnetic device designs can be avoided. Although coupling coefficients around $k \approx 0.8$ are suggested as optimal.

A substantial mass and volume saving in CI designed as explained, compared to single inductors has been demonstrated. Even a magnetic core loss reduction can be expected due to having a smaller volume core in the CI.

REFERENCES

[1] G. Spiazzi and S. Buso, "Analysis of the interleaved isolated boost converter with coupled inductors," *IEEE Transactions on Industrial Electronics*, vol. 62, no. 7, pp. 4481–4491, July 2015.

[2] Po-Wa Lee, Yim-Shu Lee, D. K. W. Cheng, and Xiu-Cheng Liu, "Steady-state analysis of an interleaved boost converter with coupled inductors," *IEEE Transactions on Industrial Electronics*, vol. 47, no. 4, pp. 787–795, Aug 2000.

[3] A. Mostaan, J. Yuan, Y. P. Siwakoti, S. Esmaeili, and F. Blaabjerg, "A trans-inverse coupled-inductor semi-sepic dc/dc converter with full control range," *IEEE Transactions on Power Electronics*, vol. 34, no. 11, pp. 10 398–10 402, Nov 2019.

[4] Y. Liu, G. Chen, Y. Hu, L. Huang, and X. Qing, "Magnetic coupling branch based dual-input/output dc-dc converters with improved cross-regulation and soft-switching operation," *IEEE Transactions on Industrial Electronics*, pp. 1–1, 2019.

[5] H. Moradisizkoohi, N. Elsayad, and O. A. Mohammed, "An integrated interleaved ultra high step-up dc-dc converter using dual cross-coupled inductors with built-in input current balancing for electric vehicles," *IEEE Journal of Emerging and Selected Topics in Power Electronics*, pp. 1–1, 2019.

[6] S. Senini and P. J. Wolfs, "The coupled inductor filter: analysis and design for ac systems," *IEEE Transactions on Industrial Electronics*, vol. 45, no. 4, pp. 574–578, Aug 1998.

[7] R. S. Balog and P. T. Krein, "Coupled-inductor filter: A basic filter building block," *IEEE Transactions on Power Electronics*, vol. 28, no. 1, pp. 537–546, Jan 2013.

[8] H. Liu and D. Zhang, "Design approach for coupled inductor filter in low-current-ripple input/output boost converter," in *2016 IEEE International Conference on Power and Renewable Energy (ICPRE)*, Oct 2016, pp. 165–171.

[9] P. Pérol, "An efficient low cost modular power system for fully regulated bus in low earth orbit applications," in *Space Power, Proceedings of the Sixth European Conference, 6-10 May.*, E. S. Agency, Ed., vol. SP-502, 2002 in Porto, Portugal., p. 375.

[10] H. Qunhai, Y. Jingyuan, W. Lixin, and W. Tongzhen, "Research on a new bidirectional dc-dc topology for space applications," in *2017 12th IEEE Conference on Industrial Electronics and Applications (ICIEA)*, June 2017, pp. 1686–1690.

[11] M. Santos, H. Ribeiro, M. Martins, and J. Guilherme, "Switch mode power supply design constraints for space applications," in *Proc. 2007 Conference on Telecommunicatios, Peniche*.

[12] G. F. Volpi, "Integrating power electronic system in space application: Limitation due to a harsh environment," in *4th International Conference on Integrated Power Systems*, June 2006, pp. 1–6.

[13] H. Kosai, S. Mcneal, A. Page, B. Jordan, J. Scofield, and B. Ray, "Characterizing the effects of inductor coupling on the performance of an interleaved boost converter," vol. 2009, 01 2009.

[14] L. Mohammadian and E. Babaei, "Investigating the effect of inductor coupling on intrinsic stability of cuk converter," in *IECON 2016 - 42nd Annual Conference of the IEEE Industrial Electronics Society*, Oct 2016, pp. 1359–1364.

[15] E. Sanchis-Kilders, A. Ferreres, J. L. Gasent-blesa, E. Maset, V. Esteve, J. Jordan, and J. B. Ejea, "Stability improvement of isolated multiple-output dc/dc converter using coupled inductors," *IEEE Transactions on Aerospace and Electronic Systems*, vol. 52, no. 4, pp. 1644–1653, August 2016.

[16] H. N. Nagaraja, D. Kastha, and A. Petra, "Design principles of a symmetrically coupled inductor structure for multiphase synchronous buck converters," *IEEE Transactions on Industrial Electronics*, vol. 58, no. 3, pp. 988–997, March 2011.

[17] G. Di Capua and N. Femia, "A critical investigation of coupled inductors sepic design issues," *IEEE Transactions on Industrial Electronics*, vol. 61, no. 6, pp. 2724–2734, June 2014.
[18] L. Dixon, "Coupled filter inductors in multi-output buck regulators," in *Texas Instruments*, 2003.
[19] S. Sau, S. P. Nikam, and B. G. Fernandes, "Coupled inductor based regenerative cascaded multicell converter for drives with multilevel voltage operation at both input and output sides," *IEEE Transactions on Industrial Electronics*, vol. 67, no. 1, pp. 147–158, Jan 2020.
[20] S. Gao, Y. Wang, and D. Xu, "A high frequency high voltage gain coupled-inductor boost circuit based on planar component," in *2018 IEEE Industry Applications Society Annual Meeting (IAS)*, Sep. 2018, pp. 1–5.
[21] N. Lecic, G. Stojanovic, S. Djuric, and E. Laboure, "Design and analysis of planar symmetric six-phase coupled inductors," *IEEE Transactions on Magnetics*, vol. 51, no. 6, pp. 1–8, June 2015.
[22] S. Ćuk and Z. Zhang, "Coupled-inductor analysis and design," in *1986 17th Annual IEEE Power Electronics Specialists Conference*, June 1986, pp. 655–665.
[23] T. Kang, B. Chae, T. Kang, and Y. Suh, "Design of coupled inductor for minimum inductor current ripple in rapid traction battery charger systems," in *2014 IEEE Energy Conversion Congress and Exposition (ECCE)*, Sep. 2014, pp. 358–364.
[24] T. Kang and Y. Suh, "Optimized coupling factor design of multiple-phase coupled inductor for minimum inductor current ripple operation in ev charger systems," in *2017 IEEE 3rd International Future Energy Electronics Conference and ECCE Asia (IFEEC 2017 - ECCE Asia)*, June 2017, pp. 1178–1183.
[25] T. Kang, J. Lee, and Y. Suh, "Design of optimized coupling factor for minimum inductor current ripple in dc-dc converter using multi-winding coupled inductor," in *2019 10th International Conference on Power Electronics and ECCE Asia (ICPE 2019 - ECCE Asia)*, May 2019, pp. 1–8.
[26] A. F. Witulski, "Introduction to modeling of transformers and coupled inductors," *IEEE Transactions on Power Electronics*, vol. 10, no. 3, pp. 349–357, May 1995.
[27] J. Zakis, D. Vinnikov, and L. Bisenieks, "Some design considerations for coupled inductors for integrated buck-boost converters," in *2011 International Conference on Power Engineering, Energy and Electrical Drives*, May 2011, pp. 1–6.
[28] Z. Dang and J. A. Abu Qahouq, "Permanent-magnet coupled power inductor for multiphase dc–dc power converters," *IEEE Transactions on Industrial Electronics*, vol. 64, no. 3, pp. 1971–1981, March 2017.
[29] M. Hagemeyer, F. Schafmeister, and J. Böcker, "Coupled inductor design for interleaved high-current dc-dc converters," in *2018 21st International Conference on Electrical Machines and Systems (ICEMS)*, Oct 2018, pp. 2316–2321.
[30] D. Gilabert, E. Sanchis-Kilders, P. J. Martínez, E. Maset, A. Ferreres, and V. Esteve, "Zero ripple current with coupled inductors in continuous conduction mode under pwm signals," *IEEE Journal of Emerging and Selected Topics in Power Electronics*, pp. 1–1, 2020.
[31] S. Cuk, "Coupled inductor and integrated magnetics techniques in power electronics," in *Telecommunications Energy Conference, 1983. INTELEC '83. Fifth International*, Oct 1983, pp. 269–275.
[32] P.-L. Wong, P. Xu, P. Yang, and F. C. Lee, "Performance improvements of interleaving vrms with coupling inductors," *IEEE Transactions on Power Electronics*, vol. 16, no. 4, pp. 499–507, July 2001.
[33] D. Gilabert, E. S. Kilders, V. Esteve, A. Ferreres, J. B. Ejea, E. Maset, J. Jordan, and E. J. Dede, "Measuring coupling coefficient of windings with dissimilar turns' number or tight coupling using resonance," *IEEE Transactions on Power Electronics*, vol. 33, no. 11, pp. 9790 – 9802, March 2018.

David Gilabert received the BSc and MSc degree in Electronic Engineering from the University of Valencia, Spain, in 2014. He is currently working towards his PhD on complex coupled inductors at the University of Valencia. He is also a member of the Laboratory of Industrial Electronics and Instrumentation. The research interests include high-frequency magnetics and space power electronics.

Esteban Sanchis-Kilders (M'00-SM'14) was born in Valencia, Spain, in 1967. He received the MSc and the PhD degree from the University of Valencia, Spain, in 1990 and 1997, respectively. After two years with the Power Conditioning Section of the European Space Agency (The Netherlands) he joined the Lab of Industrial Electronics and Instrumentation of the University of Valencia, where he is Full Professor. His research interests are space power electronics, magnetism and industrial applications.

Pedro J. Martínez was born in Villarrobledo, Spain, in 1992. He received the BSc and MSc degrees in electronic engineering from the University of Valencia in 2014 and 2015, respectively, where he is currently pursuing the PhD degree in reliability of GaN HEMT. Since 2014, he has been a member of the Lab of Industrial Electronics and Instrumentation. His research interest include electronic power devices characterization, reliability and space power electronics.

Enrique Maset (M'00) was born in Xàtiva, Spain, in October 1965. He received the MSc and PhD degrees in physics from the University of Valencia, Spain, in 1988 and 1993, respectively. He is Associate Professor in the Department of Electronic Engineering at the University of Valencia, Spain, where he is also a member of the Lab of Industrial Electronics and Instrumentation. His main research areas are space power electronics and characterization of electronic power devices.

Agustín Ferreres was born in Sant Mateu, Spain, in 1963. He received the MSc degree in physics and the PhD degree in electronic engineering from the University of Valencia, Spain, in 1993 and 1999, respectively. He was two years with the R+D Department of GH Industrial S.A. and in 1995, he joined the Lab of Industrial Electronics and Instrumentation of University of Valencia, where he is Associate Professor. His research interests include space power electronics and industrial applications.

Vicente Esteve (M'03-SM'14) was born in Valencia, Spain, in 1961. He received the MSc and PhD degrees from the University of Valencia, Spain, in 1986 and 1999, respectively. He is Associate Professor at the University of Valencia and is a member of the Lab of Industrial Electronics and Instrumentation. His research activities include high-frequency rectifiers and high-power inverters for induction heating.